ACS APPLIED MATERIALS & INTERFACES

www.acsami.org

Research Article

Suppressing the Photocatalytic Activity of Zinc Oxide Electron-Transport Layer in Nonfullerene Organic Solar Cells with a Pyrene-Bodipy Interlayer

Anastasia Soultati, Apostolis Verykios, Stylianos Panagiotakis, Konstantina-Kalliopi Armadorou, Muhammad Irfan Haider, Andreas Kaltzoglou, Charalampos Drivas, Azhar Fakharuddin, Xichang Bao, Chunming Yang, Abd. Rashid bin Mohd Yusoff, Evangelos K. Evangelou, Ioannis Petsalakis, Stella Kennou, Polycarpos Falaras, Konstantina Yannakopoulou, George Pistolis, Panagiotis Argitis, and Maria Vasilopoulou*

Cite This: *ACS Appl. Mater. Interfaces* 2020, 12, 21961−21973

Read Online

ACCESS | Metrics & More | Article Recommendations | Supporting Information

ABSTRACT: Organic solar cells based on nonfullerene acceptors have recently witnessed a significant rise in their power conversion efficiency values. However, they still suffer from severe instability issues, especially in an inverted device architecture based on the zinc oxide bottom electron transport layers. In this work, we insert a pyrene-bodipy donor−acceptor dye as a thin interlayer at the photoactive layer/zinc oxide interface to suppress the degradation reaction of the nonfullerene acceptor caused by the photocatalytic activity of zinc oxide. In particular, the pyrene-bodipy-based interlayer inhibits the direct contact between the nonfullerene acceptor and zinc oxide hence preventing the decomposition of the former by zinc oxide under illumination with UV light. As a result, the device photostability was significantly improved. The π−π interaction between the nonfullerene acceptor and the bodipy part of the interlayer facilitates charge transfer from the nonfullerene acceptor toward pyrene, which is followed by intramolecular charge transfer to bodipy part and then to zinc oxide. The bodipy-pyrene modified zinc oxide also increased the degree of crystallization of the photoactive blend and the face-on stacking of the polymer donor molecules within the blend hence contributing to both enhanced charge transport and increased absorption of the incident light. Furthermore, it decreased the surface work function as well as surface energy of the zinc oxide film all impacting in improved power conversion efficiency values of the fabricated cells with champion devices reaching values up to 9.86 and 11.80% for the fullerene and nonfullerene-based devices, respectively.

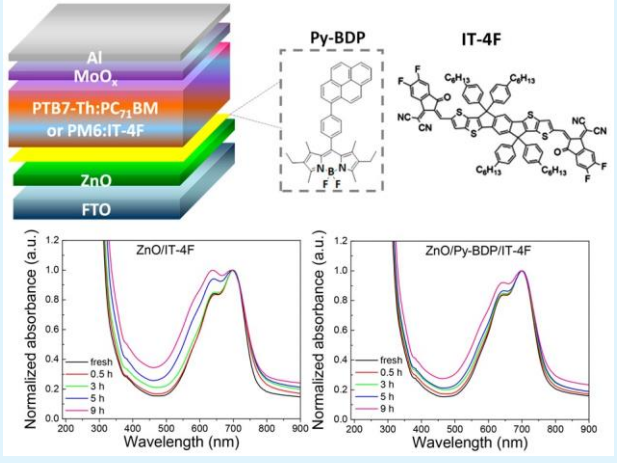

KEYWORDS: *organic solar cells, zinc oxide, nonfullerene acceptors, photocatalytic activity, pyrene, bodipy, photostability*

1. INTRODUCTION

Organic solar cells (OSCs) have attracted tremendous research interest in the past decades because of their compatibility with lightweight flexible substrates in combination with their simple and low-cost manufacturing via solution-processing.[1−5] OSCs based on the bulk heterojunction (BHJ) architecture, consisting of blends of a polymer donor with a fullerene acceptor have been the subject of intense research efforts for about two decades, leading to power conversion efficiency (PCE) values from about 1% to ∼10.4% in single-junction and of ∼15% in tandem OSCs.[6−8] However, recent developments on nonfullerene acceptors (NFAs) have led to a rapid increase in PCEs, with values of ∼17.1% in ternary blend single-junction cells[9] and ∼17.3% in double-junction tandem OSCs.[10] The salient features of NFAs such as attractive optical properties, resilience to environmental oxidation and facile tunability of electronic energy levels make them ideal candidates for high-performance OSCs.[11−16]

Besides the properties of the photoactive layer, interfacial layers with excellent charge extraction/transport capability also

Received: February 26, 2020
Accepted: April 21, 2020
Published: May 4, 2020

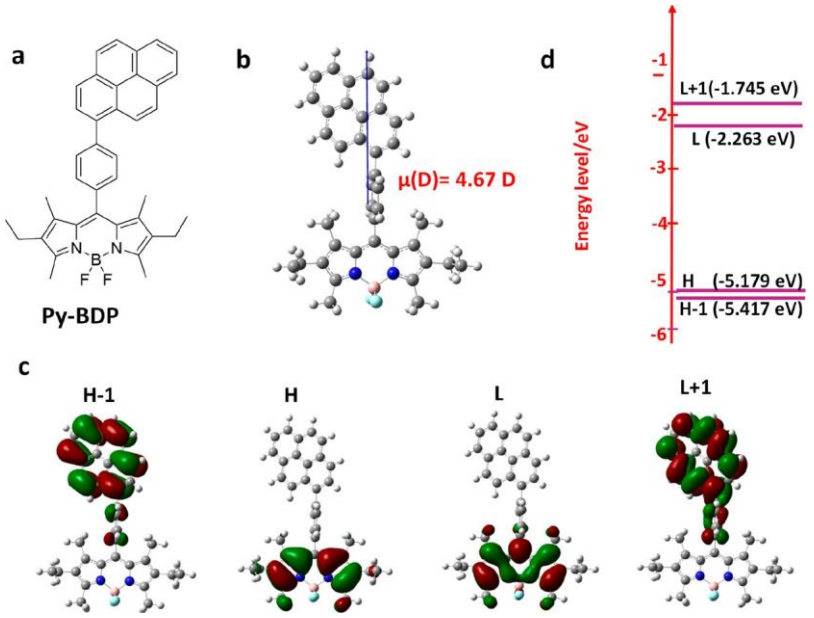

Figure 1. (a) Molecular structure and (b) optimal geometry along with calculated dipole moment of Py-BDP dye. (c) DFT calculated frontier molecular orbital (HOMO, LUMO) and (d) energy levels of Py-BDP molecule.

play a crucial role in improving the performance of OSCs.[17−24] Although they do not interfere with the photon-to-electron-conversion efficiency process, they facilitate charge transport toward the collection of electrodes and improve charge collection efficiency, control interfacial recombination losses during charge transfer process, and contribute to device stability.[20−22] Transition metal oxides, especially titanium dioxide (TiO_2) and zinc oxide (ZnO), have been widely applied as the bottom electron transport layers (ETLs) in the inverted device architecture because of their sufficient transmittance within the visible spectral range, adequate n-type electronic conductivity and simple film formation via solution-processing.[25−33] However, ZnO exhibits intense photocatalytic activity within the UV spectral region due to the action of photoinduced charge carriers and resulting reactive oxygen species (ROS, e.g., hydroxyl radicals).[34,35] Upon illumination with UV light, the defect-rich ZnO induces chemical reactions at the ETL/absorber interface causing the decomposition of NFA absorber layer.[36,37] Recently, Jiang et al. demonstrated severe degradation of one of the most efficient NFAs, namely, 3,9-bis(2-methylene-((3-(1,1-dicyanomethylene)-6,7-difluoro)-indanone))-5,5,11,11-tetrakis(4-hexylphenyl)-dithieno[2,3-d:2′,3′-d′]-s-indaceno[1,2-b:5,6-b′]-dithiophene (IT-4F), caused by the photocatalytic activity of ZnO.[37] One approach to mitigate this interfacial degradation is to dope the ZnO layer with appropriate elements such as lithium cations (Li^+) as previously demonstrated by our group.[32] Moreover, surface defects passivation of ZnO through the insertion of appropriate interlayers at the ETL/photoactive layer interface is also considered beneficial.[38] Organic molecules such as self-assembled monolayers (SAMs),[39,40] ionic liquids,[41−43] and functionalized fullerenes,[44−47] with tunable energetics such as deep-lying highest occupied molecular orbital (HOMO) and appropriate lowest unoccupied molecular orbital (LUMO), are commonly used as interlayers between the ZnO ETL and the photoactive blend. They also improve electron extraction toward cathode and effectively block holes reaching the opposite metal electrode, hence reducing the device leakage current. Additionally, they affect the surface energy of ZnO, thus dictating the nanomorphology of the photoactive layer deposited over it.[48,49] However, many of those materials contain amino groups in their structure in order to enable the formation of large negative interfacial dipoles that lead to a downward shift of the vacuum level at the respective interface.[50,51] This, unfortunately, has also proven detrimental for the stability of NFAs. In particular, Hu et al. have recently demonstrated that nucleophilic amino groups react with the carbonyl (C=O) moiety of ITIC acceptors thus destroying their electronic structure and suppressing the intramolecular charge transfer ability of ITIC molecules.[36]

To overcome the above limitations, we here propose the application of a pyrene-bodipy molecular dye, termed hereafter as Py-BDP, as an ultrathin interlayer at the ZnO/IT-4F interface to mitigate the ZnO mediated photocatalytic degradation of OSCs. The selection of Py-BDP dye was motivated by the absence of amino groups and its donor−acceptor (D-A) nature that is expected to facilitate intramolecular charge transfer. The devices based on Py-BDP exhibited significant resistance to light-induced degradation compared to pristine ZnO counterparts. Moreover, the insertion of a ∼4 nm thin Py-BDP interlayer resulted in a 0.3 eV decrease in the work function (W_F) of ZnO ETL and altered its surface energy. The latter significantly improved the nanomorphology and increased the degree of crystallinity of the photoactive blend coated on top of it while also enhancing the face-on stacking of the polymer donor molecules within the blend. Consequently, a significant PCE enhancement was obtained for the Py-BDP-based devices using either fullerene acceptors (FAs) or NFAs, with champion devices reaching values up to 9.86 and 11.80%, respectively.

2. RESULTS AND DISCUSSION

Surface Properties of ZnO Coated with Pyrene- Bodipy. Figure 1a presents the molecular structure of the pyrene-bodipy dye where a phenyl unit was incorporated as a

https://dx.doi.org/10.1021/acsami.0c03147
ACS Appl. Mater. Interfaces 2020, 12, 21961−21973

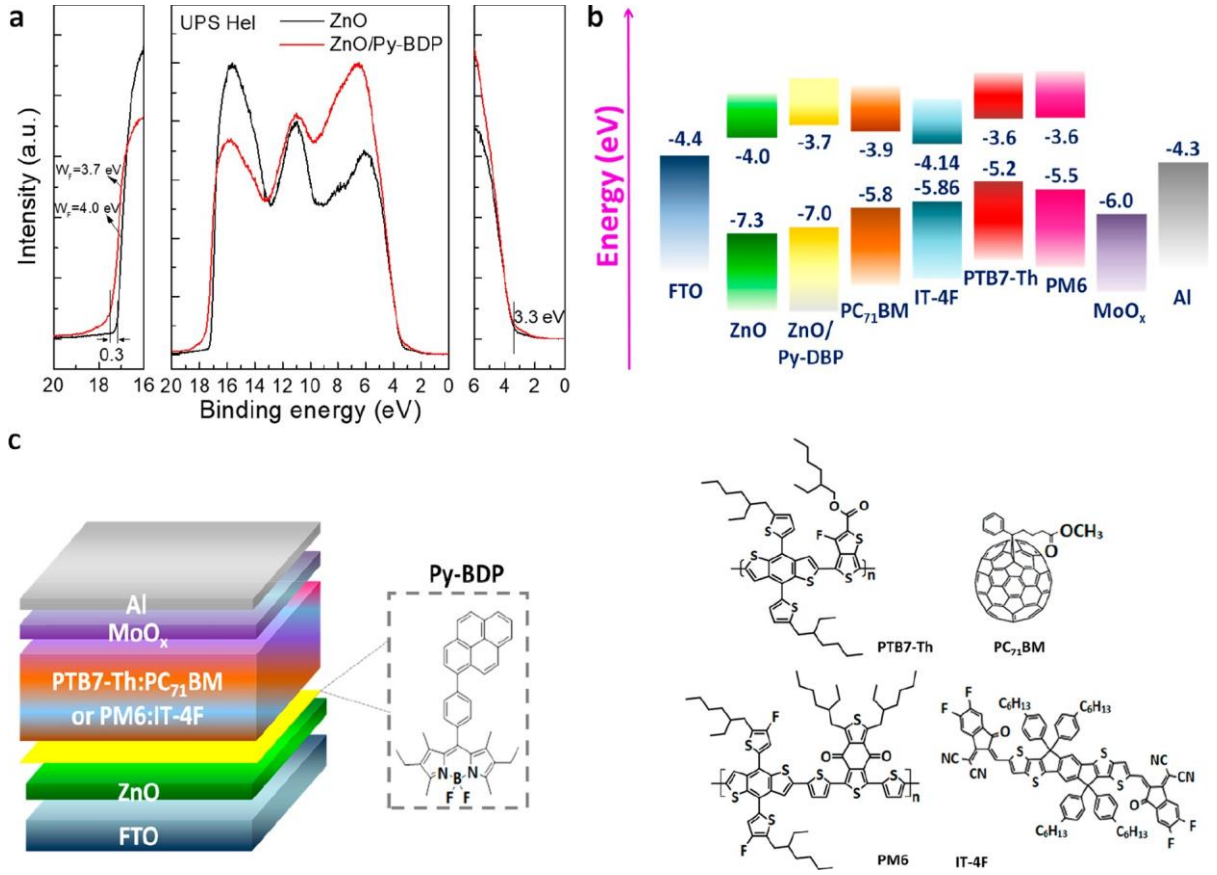

Figure 2. (a) UPS spectra (left, the high binding energy region; middle, the expanded view; right, the near Fermi level region) of pristine and Py-BDP-coated ZnO layer (on glass/FTO substrate). (b) Energy levels, considering vacuum level alignment before contact, of different layers used for the fabrication of fullerene and nonfullerene OSCs: W_F of FTO, VBM and CBM of ZnO and ZnO/Py-BDP, HOMO and LUMO levels of organic semiconductors, W_F of MoO_x and Al. (c) Device structure of fullerene and nonfullerene OSCs. In the right panel, the chemical structure of donor and acceptor materials consisting of fullerene (up) and nonfullerene (down) blends are shown.

chemical linker to enhance the intramolecular electron transfer from the pyrene donor to the bodipy acceptor fragment. The detailed synthetic procedure of Py-BDP is given in Figure S1. Density functional theory (DFT) verified that pyrene acts as the donor, whereas bodipy represents the acceptor segment of the Py-BDP molecule (Figure S2). DFT calculations also showed the influence of molecular geometry on the photophysical properties of the Py-BDP molecule (Figure 1b). It is observed that pyrene and bodipy fragments are vertically oriented to one another. The molecule exhibits a high dipole moment of 4.67 D. A large molecular dipole causes higher intramolecular charge-transfer rates.[52] The DFT calculated HOMO−1, HOMO, LUMO, and LUMO+1 orbitals and molecular energy levels of Py-BDP are shown in Figure 1c, d, respectively. It is observed that both HOMO and LUMO levels are localized on the BDP moiety. On the contrary, HOMO−1 and LUMO+1 reside on the pyrene moiety. Because of its clear donor−acceptor (or else "push−pull" character) and large molecular dipole moment, Py-BDP is expected to allow for fast intramolecular electron-transfer rates, which could play a role in OSCs by facilitating electron transfer from the absorber toward ZnO.

The ZnO films used as the bottom ETLs were obtained through a solution-processed deposition method described in the Experimental Section. They exhibited small amount of surface defects and smooth surface morphology as indicated by steady-state photoluminescence (PL) measurements and atomic force microscopy (AFM) images, respectively, shown in Figure S3. We then investigated the influence of inserting a thin (~4 nm) Py-BDP interlayer, derived from a methanol solution with a concentration of 0.35 mg mL^{-1} that gave the best device performance, on the optoelectronic properties of ZnO ETLs. Figure S4 depicts the UV−vis transmittance and absorption spectra of ZnO without and with the thin dye overlayer. It is observed that pristine and Py-BDP-coated ZnO substrates exhibit similar transmittance and absorption properties with negligible absorption within the visible. This suggests that the insertion of Py-BDP interlayer does not block sunlight reaching absorber layer which would otherwise limit current density. The Tauc plots derived from the absorption spectra (Figure S5) showed the same energy bandgap value (E_g = 3.25 eV). In contrast, ultraviolet photoelectron spectroscopy (UPS) measurements, presented in Figure 2a, revealed significant W_F reduction of about 0.3 eV upon coating ZnO with Py-BDP. The lower W_F of ZnO/Py-BDP bilayer is expected to induce a favorable vacuum level downward shift at the photoactive layer/cathode interface, leading to a reduction in the barrier for electron extraction thus improving the device performance. The corresponding energy level diagram of the fullerene (using a poly[4,8-bis(5-(2-ethylhexyl)thiophen-2-yl)benzo[1,2-*b*;4,5-*b*′]dithiophene-2,6-diyl-*alt*-(4-(2-ethylhexyl)-3-fluorothieno-[3,4-*b*]thiophene-)-(2-carboxylate-2−6-diyl)]:phenyl-C_{71}-butyric acid methyl ester (PTB7-Th:$PC_{71}BM$) blend) and nonfullerene (using a poly[(2,6-(4,8-bis(5-(2-ethylhexyl-3-

https://dx.doi.org/10.1021/acsami.0c03147
ACS Appl. Mater. Interfaces 2020, 12, 21961−21973

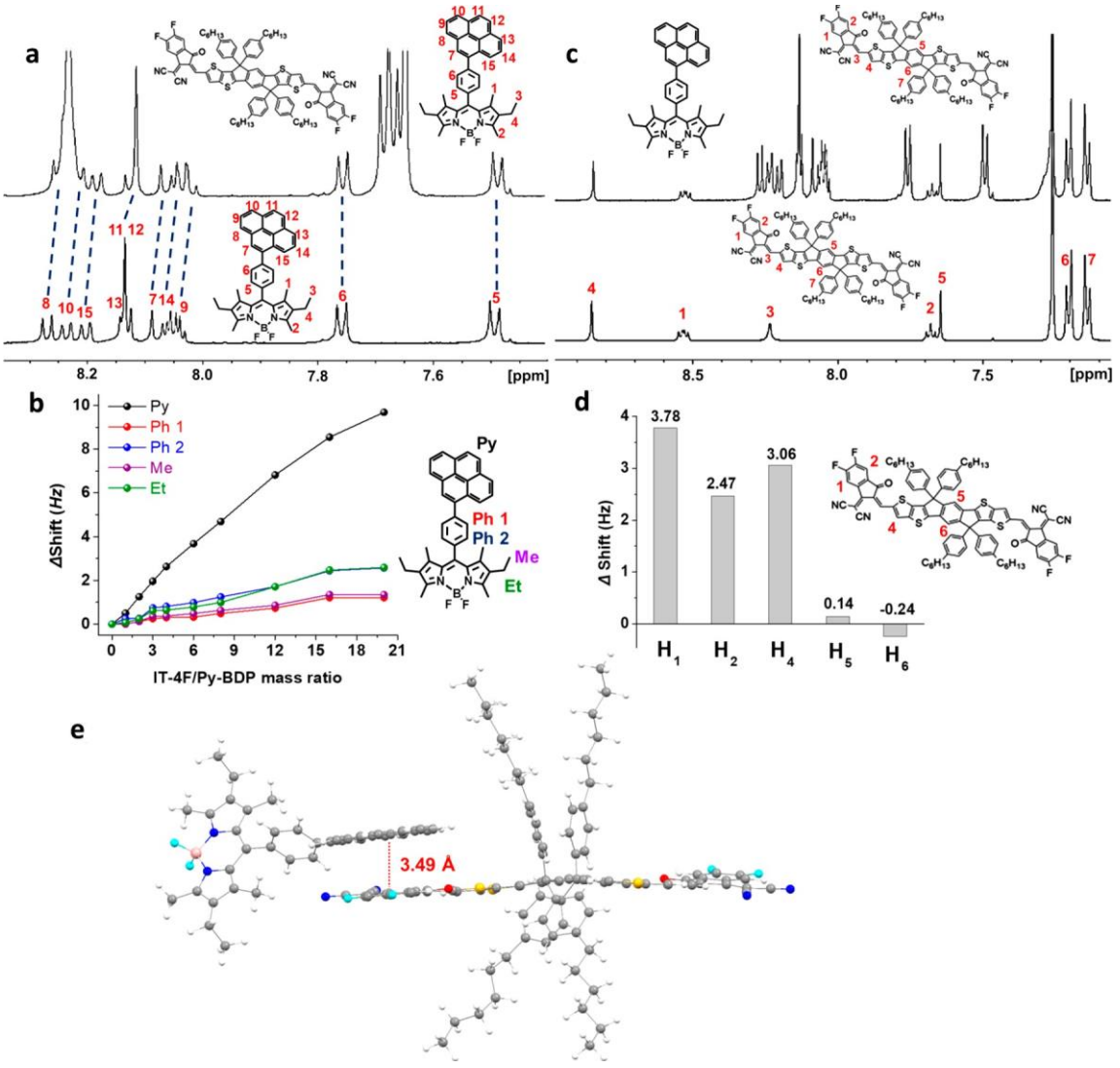

Figure 3. (a) Partial ^{1}H NMR spectra (500 MHz, $CDCl_3$, 298 K) of Py-BDP (0.5 mg/mL) before and after addition of IT-4F (10.0 mg/mL). (b) Diagram of chemical shift changes (Hz) of H_{12} of pyrene (Pyr), phenyl (Ph), and aliphatic (Me, Et) protons of Py-BDP, upon gradual addition of IT-4F. The Pyr proton signals undergo the highest chemical shift changes (shielding). (c) Partial ^{1}H NMR (500 MHz, $CDCl_3$, 298 K) spectra of IT-4F (0.5 mg/mL) before and after addition of Py-BDP (0.5 mg/mL). (d) Diagram of chemical shift changes (shielding) in Hz of protons of IT-4F upon addition of Py-BDP. (e) Schematic illustration of optimized geometries of Py-BDP and IT-4F π−π interactions based on NMR data. Hydrogen, carbon, nitrogen, oxygen, fluorine, sulfur, and boron correspond to light gray, gray, blue, red, light blue, orange, and pink spheres, respectively.

fluoro)thiophen-2-yl)-benzo[1,2-b:4,5-b′]dithiophene))-*alt*-(5,5-(1′,3′-di-2-thienyl-5′,7′-bis(2-ethylhexyl)benzo[1′,2′-c:4′,5′-c′]dithiophene-4,8-dione)]:3,9-bis(2-methylene-((3-(1,1-dicyanomethylene)-6,7-difluoro)-indanone))-5,5,11,11-tetrakis(4-hexylphenyl)-dithieno[2,3-d:2′,3′-d′]-s-indaceno-[1,2-b:5,6-b′]dithiophene (PM6:IT-4F) blend) OSCs based on both pristine and Py-BDP-coated ZnO ETLs is depicted in Figure 2b. The W_F values of FTO, MoO_x, and Al as well as the HOMO and LUMO levels of organic semiconductors used in this study were taken from the literature.[53,54] The valence band maximum (VBM) of ZnO and ZnO coated with Py-BDP were calculated through adding the binding energy (BE) of the valence band onset (3.3 eV in both cases) to the W_F values (4.0 and 3.7 eV, respectively) estimated from the secondary electron cutoff region of the UPS spectra. The conduction band minima (CBM) were estimated by subtracting the value of E_g (which was taken equal to 3.3 eV for simplicity). It is observed that the CBM of ZnO/Py-BDP locates at about 3.7 eV, which is above the LUMOs of $PC_{71}BM$ and IT-4F. However, the formation of a large negative dipole at the ZnO/Py-BDP/photoactive blend interface strongly enhances the device built-in field and practically sweeps electrons from the photoactive blend toward cathode. Moreover, we found change in surface energy of ZnO upon coating the Py-BDP dye. Figure S6a, b show the contact angle measurements of a droplet of deionized water and diiodomethane taken on bare and Py-BDP-coated ZnO. The calculated surface energy in each case is shown in Table S1. Interestingly, the insertion of the thin Py-BDP interlayer on top of ZnO changes the surface properties of the latter, resulting in more hydrophobic surface and in reduced surface energy. The significant increase in water contact angle on ZnO/Py-BDP bilayer indicates that the amphiphilic bodipy is preferentially attached to the ZnO surface, whereas the hydrophobic pyrene is oriented on the

https://dx.doi.org/10.1021/acsami.0c03147
ACS Appl. Mater. Interfaces 2020, 12, 21961−21973

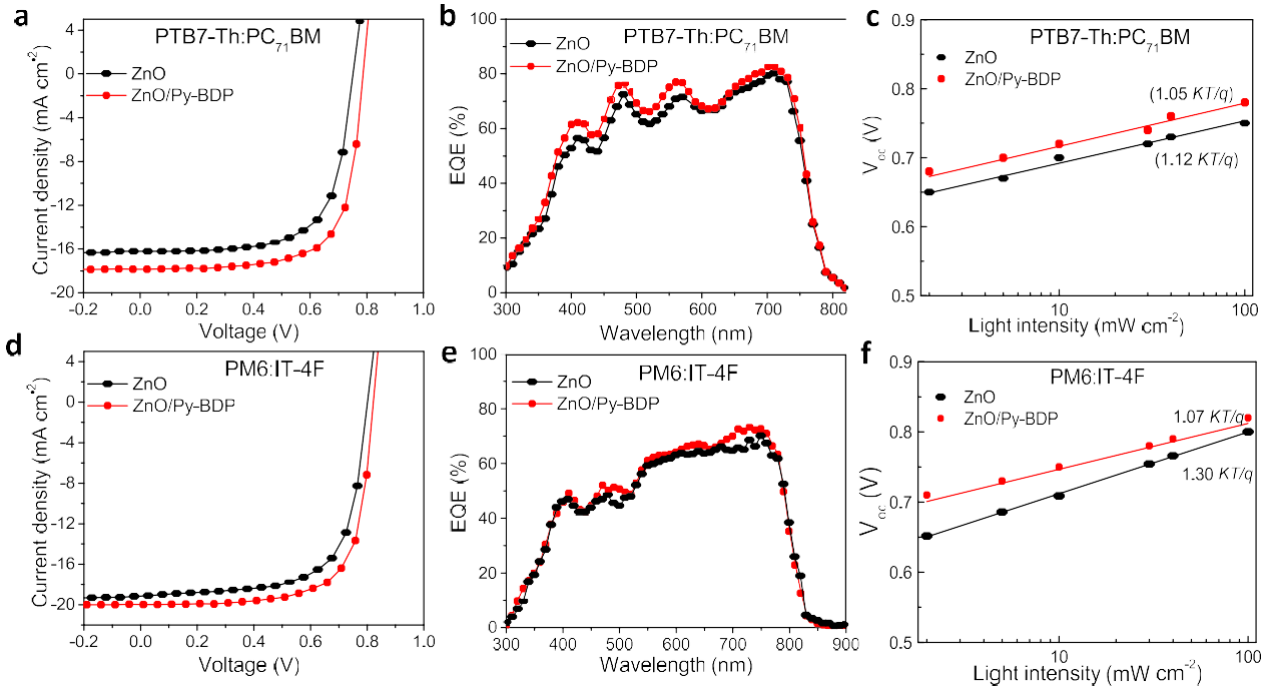

Figure 4. (a) Current density versus voltage ($J-V$) characteristic curves measured under AM 1.5G illumination and (b) EQE measurements of fullerene OSCs based on PTB7-Th:$PC_{71}BM$ layer using pristine and Py-BDP-modified ZnO as ETLs. (c) Plots of V_{oc} versus intensity of light illumination of the fullerene OSCs with either ZnO or ZnO/Py-BDP ETL. (d) $J-V$ characteristic curves taken under illumination and (e) EQE measurements of nonfullerene (PM6:IT-4F) OSCs. (f) Plots of V_{oc} versus intensity of light illumination of the nonfullerene OSCs with either ZnO or ZnO/Py-BDP ETL.

Table 1. Device Characteristics of Fullerene OSCs with Structure Glass/FTO/ZnO or ZnO/Py-BDP/PTB7-Th:$PC_{71}BM$/MoO_x/Al[a]

ETL	$J_{sc,max}$($J_{sc,ave}$) (mA cm^{-2})	$V_{oc,max}$ ($V_{oc,aver}$) (V)	FF_{max} (FF_{ave})	PCE_{max} (PCE_{ave}) (%)	R_s (Ω cm^2)	R_{sh} (Ω cm^2)
ZnO	16.19(15.88 ± 0.22)	0.75(0.74 ± 0.1)	0.69(0.67 ± 0.2)	8.38(7.87 ± 0.21)	3.0	1300
ZnO/Py-BDP	17.83(17.24 ± 0.19)	0.79(0.78 ± 0.1)	0.70(0.69 ± 0.1)	9.86(9.28 ± 0.21)	1.5	1980

[a]Average values and standard deviations were extracted from a batch of 16 different devices fabricated under identical conditions.

opposite site toward the photoactive blend in the complete OSC structure. The device architecture and the chemical structure of the donor and acceptor materials are presented in Figure 2c.

Interaction between the Nonfullerene Acceptor and Pyrene-Bodipy. Furthermore, we used proton nuclear magnetic resonance (^{1}H NMR) spectroscopy experiments to probe the interactions between Py-BDP and IT-4F molecules in solution. In the presence of IT-4F all ^{1}H NMR signals of the pyrene part of Py-BDP are shielded (Figure 3a, max shift $\Delta\delta$ = 10 Hz), whereas the other protons almost keep constant as also shown in the titration experiment of Figure 3b and Figure S7. The titration data were fitted with a suitable nonlinear equation for 1:1 association (eq 1) and the value of the equilibrium constant was calculated (K = 103 ± 5 M^{-1}, R^2 = 0.996, Figure S8). Reversely, comparison of the ^{1}H NMR spectra of IT-4F (0.5 mg/mL) before and after the addition of Py-BDP (0.5 mg/mL) (Figure 3c) revealed that only H_1, H_2, and H_3 of IT-4F were shielded by 3.78, 2.47, and 3.06 Hz, respectively (Figure 3d). These observations can be explained by the establishment of π−π interactions between the pyrene part of Py-BDP and the outer planar dicyanomethylene-difluoroindanone moieties of IT-4F, whereas the other parts of the molecules remain uninvolved. Dilution experiments suggested that the individual molecules do not self-assemble into aggregated structures (Figures S9 and S10). To evaluate the binding model via π−π interactions, we employed the Molecular Mechanics module of Avogadro 1.20. After optimization the distance of π−π interactions between the approaching components of Py-BDP and IT-4F molecules was calculated at 3.49 Å (Figure 3e). Similar interactions beetween pyrene derivatives and other aromatic systems have been reported previously.[55] A binding model with C−H···π interactions was calculated as energetically less favored. The NMR results show close proximity of the interacting Py-BDP and IT-4F molecules even in solution state. The close approach in the solid state could enable efficient intermolecular charge transfer from IT-4F to pyrene (donor) segment of Py-BDP. This is followed by intramolecular charge transfer to bodipy (acceptor) segment and then to ZnO ETL. Such efficient electron transfer from IT-4F to ZnO through Py-BDP interlayer was further supported by PL measurements taken in IT-4F films deposited on both pristine and Py-BDP-coated ZnO (on FTO/glass substrates) (Figure S11). The characteristic emission of IT-4F was significantly quenched when inserting the Py-BDP between the acceptor's film and the ZnO substrate.

Organic Solar Cell Performance. We next investigated the effect of inserting Py-BDP at the ZnO/photoactive blend interface on the device performance. Figure 4a, d shows the

https://dx.doi.org/10.1021/acsami.0c03147
ACS Appl. Mater. Interfaces 2020, 12, 21961−21973

Table 2. Device Characteristics of Nonfullerene OSCs with Structure Glass/FTO/ZnO or ZnO/Py-BDP/PM6:IT-4F/MoO_x/Al[a]

ETL	$J_{sc,max}$ ($J_{sc,ave}$) (mA cm^{-2})	$V_{oc,max}$ ($V_{oc,aver}$) (V)	FF_{max} (FF_{aver})	PCE_{max} (PCE_{ave}) (%)	R_s (Ω cm^2)	R_{sh} (Ω cm^2)
ZnO	19.14(18.92 ± 0.21)	0.80(0.79 ± 0.1)	0.68(0.67 ± 0.1)	10.41(10.01 ± 0.19)	2.6	892
ZnO/Py-BDP	19.98(19.79 ± 0.21)	0.82(0.81 ± 0.1)	0.72(0.70 ± 0.1)	11.80(11.22 ± 0.19)	1.4	2112

[a]Average values and standard deviations were extracted from a batch of 16 different devices fabricated under identical conditions.

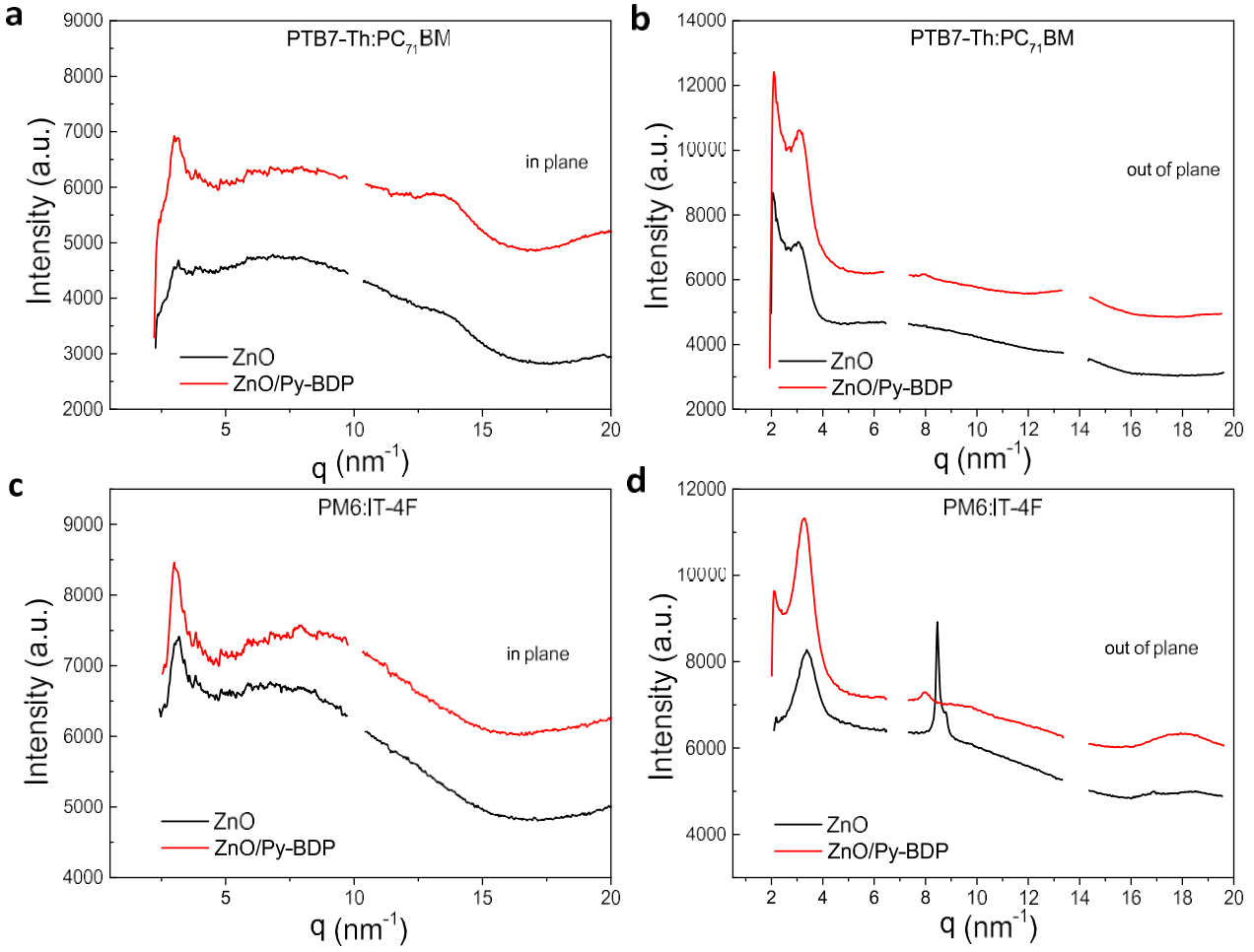

Figure 5. 1D GIWAXS patterns along (a, c) in-plane and (b, d) out-of-plane directions, respectively, for (a, b) PTB7-Th:PC_{71}BM and (c, d) PM6:IT-4F coated on top of pristine and Py-BDP-modified ZnO substrates.

current density−voltage characteristic curves of the best-performing fullerene- and non-fullerene-based OSCs, respectively, using ZnO/Py-BDP as ETLs. The photovoltaic parameters of these devices are also summarized in Tables 1 and 2 where average values extracted from a batch of 16 similar devices of each type are also included. For comparison, reference devices with pristine ZnO ETLs were also fabricated. A significant improvement in the device performance metrics was observed in Py-BDP-modified OSCs based on both PTB7-Th:PC_{71}BM and PM6:IT-4F blends, revealing the versatility of Py-BDP as an interlayer between ZnO and the photoactive layer regardless of the organic donor−acceptor blend. In the case of PTB7-Th:PC_{71}BM-based device, the reference cell based on ZnO ETL exhibited a short-circuit current density (J_{sc}) of 16.19 $mAcm^{-2}$, an open-circuit voltage (V_{oc}) of 0.75 V, and a fill factor (FF) of 0.69, leading to a PCE value of 8.38%. A 17% improvement in the device performance was obtained using ZnO/Py-BDP as ETL. This arises from an increase in all device electrical characteristics (J_{sc} of 17.83 $mAcm^{-2}$, V_{oc} of 0.79 V, and FF of 0.70, and thus a PCE of 9.86%). Similarly, PM6:IT-4F-based OSCs using the Py-BDP interlayer yielded a higher PCE value of 11.80% compared with the reference cell (PCE value of 10.41%). This 13% performance improvement derived from the simultaneous increase in J_{sc} (from 19.14 to 19.98 $mAcm^{-2}$), V_{oc} (from 0.8 to 0.82 V) and FF (from 0.68 to 0.72). Furthermore, a significant increase in the shunt (R_{sh}) resistance and a large decrease in series (R_s) of the Py-BDP-based OSCs was obtained indicating the improved quality of the electron-transport interface compared with the reference devices. Moreover, external quantum efficiency (EQE) measurements of the same devices are presented in Figure 4b and 4e for the fullerene and nonfullerene OSCs, respectively. Enhanced EQE values are observed for the Py-BDP-modified OSCs, indicating that the insertion of Py-BDP as an interlayer highly improves the photon-to-electron-conversion efficiency process. This can be related to the improvement in electron extraction as well as more efficient absorption of the incident light (Figure S12) in the ZnO/Py-

https://dx.doi.org/10.1021/acsami.0c03147
ACS Appl. Mater. Interfaces 2020, 12, 21961−21973

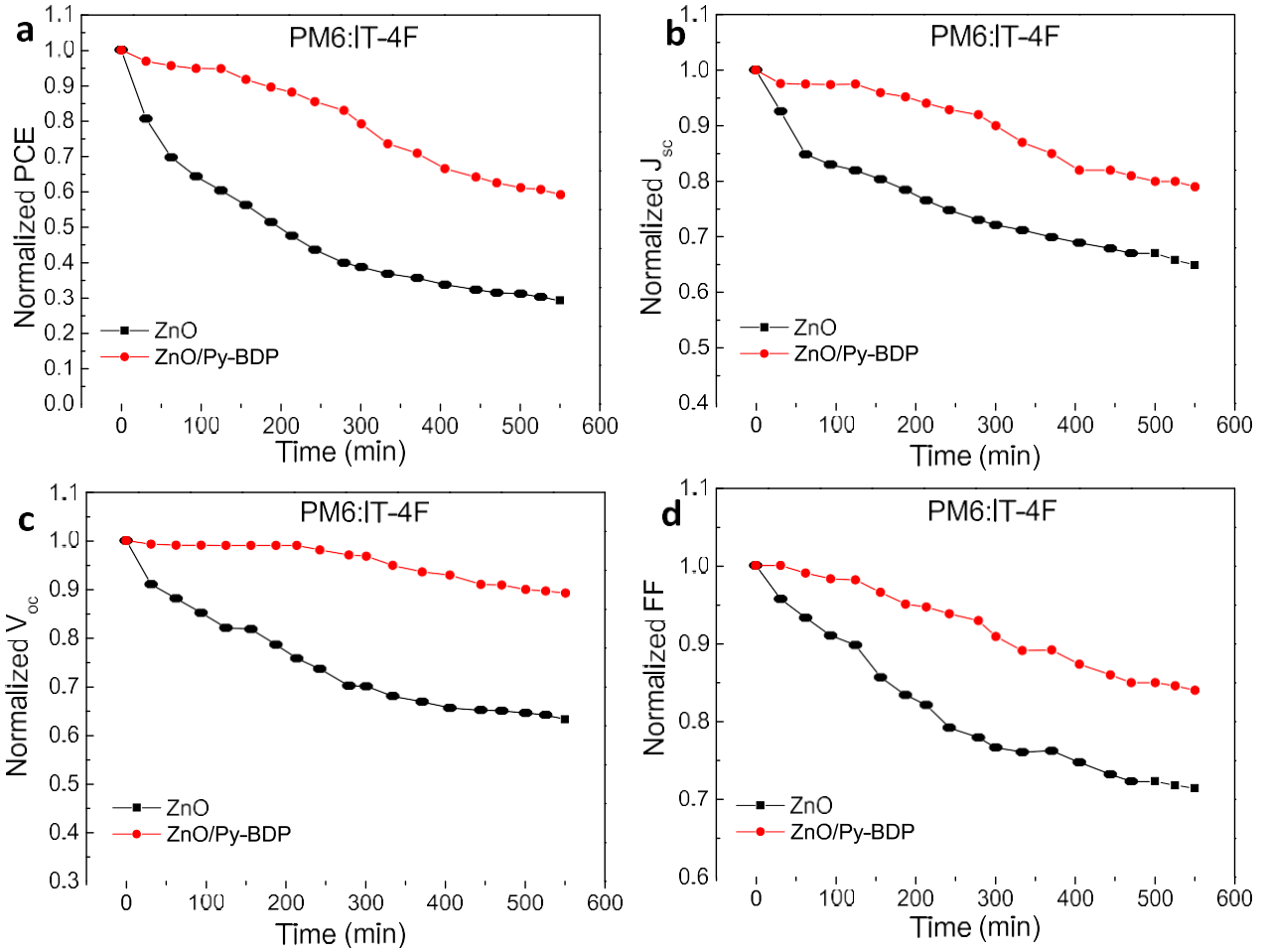

Figure 6. Photostability study: variation in (a) PCE, (b) J_{sc}, (c) V_{oc}, and (d) FF versus time of unencapsulated nonfullerene OSCs under constant AM 1.5G illumination for 9 h.

BDP-based OSCs. Figure S13 shows the $J-V$ characteristic curves in a semilogarithmic scale taken in electron only devices of both types fullerene and nonfullerene ones. The device structure was FTO/ZnO without or with Py-BDP/photoactive layer/Al, respectively. The higher electron currents achieved when using Py-BDP-modified ZnO ETLs derive from the reduced electron extraction barrier and improved light absorption. Moreover, for a deeper understanding of charge recombination mechanism in fullerene and nonfullerene OSCs using pristine and Py-BDP coated ZnO ETLs, the dependence of V_{oc} on the illumination intensity was investigated. The corresponding results are shown in Figure 4c, for fullerene and nonfullerene OSCs, respectively. The slopes of V_{oc} with respect to the light intensity were significantly decreased upon the application of Py-BDP. The slopes decrease from $1.12KT/q$ to $1.05KT/q$ and from $1.30KT/q$ to $1.07KT/q$ for the devices based on PTB7-Th:$PC_{71}BM$ and PM6:IT-4F, respectively (K is the Boltzmann constant, T the absolute temperature, and q is the elementary charge). These results suggest that trap-assisted recombination losses are suppressed in the Py-BDP-modified cells.

The improvement in electron transport and in absorption of incident light as well as overall device performance with the insertion of Py-BDP between the ZnO and the photoactive layer could be related to changes in the nanomorphology of the BHJ film deposited on top of it. Therefore, the morphological properties of PTB7-Th:$PC_{71}BM$ and PM6:IT-4F deposited on pristine and Py-BDP-modified ZnO were investigated by performing grazing-incidence wide-scanning X-ray scattering (GIWAXS) measurements. The 1D patterns of PTB7-Th:$PC_{71}BM$ blend deposited on ZnO and ZnO/Py-BDP substrates for the in-plane and out-of-plane directions are shown in Figure 5a , b, respectively. In both cases, the lamellar peak of PTB7-Th:$PC_{71}BM$ film corresponding to the (100) Bragg reflection at $q = 3.06$ nm^{-1} is clearly seen in the out-of-plane curves, in addition to the peak at $q = 3.17$ nm^{-1} in the in-plane curves.[56] Interestingly, the polymer alkyl stacking peak of the ZnO/Py-BDP/PTB7-Th:$PC_{71}BM$ sample is more intense compared with that of the ZnO/PTB7-Th:$PC_{71}BM$ indicating a higher degree of crystallinity in the blend when deposited on top of ZnO/Py-BDP. On the other hand, an increase in the intensity of the broad in-plane peak centered at ~13 nm^{-1} ($d \approx 0.48$ nm) attributed to the (220) peak of $PC_{71}BM$ was observed in the Py-BDP-modified ZnO/PTB7-Th:$PC_{71}BM$, indicating an enhancement in aggregation of $PC_{71}BM$.[57] Notably, the (010) peak at 17.3 nm^{-1} which is attributed to the $\pi-\pi$ stacking of PTB7-Th is completely absent in the in-plane pattern of the blend film on ZnO, whereas it appears, though very weak, in the pattern of the blend film on top of ZnO/Py-BDP. Similarly, the degree of crystallinity of PM6:IT-4F blend deposited on ZnO/Py-BDP substrate is also higher compared to that of the ZnO/PM6:IT-4F sample, as evidenced by the overall higher peak intensity in the former case. The lamellar peak at $q \approx 3.3$ nm^{-1} observed in the out-of-

https://dx.doi.org/10.1021/acsami.0c03147
ACS Appl. Mater. Interfaces 2020, 12, 21961−21973

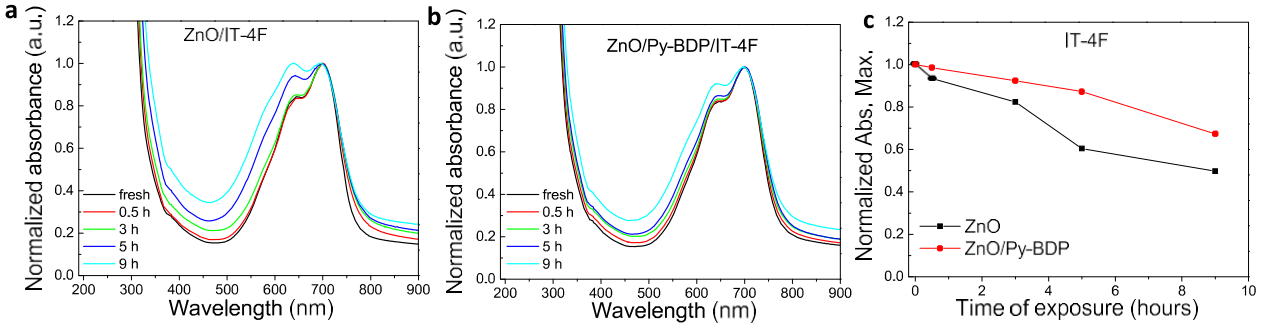

Figure 7. UV−vis absorption spectra of fresh and exposed to AM 1.5 G (1 sun) light illumination IT-4F films coated on (a) ZnO and (b) ZnO/Py-BDP substrates. (c) Absorption maximum changes of IT-4F deposited on pristine and Py-BDP-modified ZnO under AM 1.5G light exposure.

plane direction for both samples corresponding to (100) plane of PM6 is more intense for the PM6:IT-4F coated on Py-BDP-modified ZnO. A weak π−π stacking peak attributed to the (010) plane of PM6 at ∼17.8 nm^{-1} ($d \approx 0.35$ nm) also appears in this sample, indicating a weak face-on orientation.[58,59] These results present evidence that the insertion of Py-BDP at the ETL/photoactive layer interface influences the molecular ordering of the organic blend (both PTB7-Th:$PC_{71}BM$ and PM6:IT-4F) by inducing a higher degree of crystallization and face-on orientation of the polymer donor (and improved aggregation in the case of $PC_{71}BM$ acceptor). The improved π−π polymer stacking is an additional reason for the enhancement in electron transport toward the cathode in the modified devices. The improved ordering of organic blends on top of the modified ZnO could be related to the decrease in surface energy of ZnO upon Py-BDP coverage. The lower surface energy may favor the nucleation and growth of more crystalline films, as evidenced by GIWAXS measurements.

Photostability Study. One of the main goals of this work was to successfully mitigate the photocatalytic activity of ZnO on NFA, thus improving the device stability under constant illumination. From Figure 6 and Figure S14, it is evident that the intentionally unencapsulated OSCs with the Py-BDP modified ZnO ETL exhibited significantly enhanced photostability, as manifested by the slower decrease of all electrical characteristics of these devices when subjecting to continuous illumination with AM 1.5G (1 sun) light for 540 min (9 h). These measurements were performed in air at 25 °C and 40% relative humidity. For the lifetime experiment, we measured five cells of each type. It is deduced that the Py-BDP-modified OSC based on PTB7-Th:$PC_{71}BM$ blend retained 66% of the initial PCE value after 540 min of constant illumination, whereas the reference cell employing the pristine ZnO ETL retained only 24% of the initial PCE under the same time period and identical measurement conditions. Similarly, in the case of nonfullerene OSCs with the PM6:IT-4F layer on top of ZnO ETL, the PCE dropped to about 70% of its initial value. In contrast, in the Py-BDP-modified device, this drop was only 41%, after 540 min of constant AM 1.5G illumination at the same conditions (measured in air, at 25 °C and 40% relative humidity).

To understand the enhanced photostability of ZnO/Py-BDP-based OSCs, we should take into account that ZnO behaves as a photocatalyst under UV illumination and, therefore, it is possible that it decomposes the IT-4F during 1 sun illumination (that contains a small portion of UV light). This is because, under irradiation with light of energy higher than its energy gap (that is UV light), ZnO can generate electrons (e^-) in the CB and positively charged holes (h^+) in the VB. On the surface of ZnO, the photogenerated holes (h^+) will react with adsorbed H_2O to form hydroxyl radicals ($OH^•$). The photogenerated electrons (e^-) can be captured by O_2 (that is always adsorbed on the oxide's surface) to generate superoxide radicals ($O_2^{•-}$), which further generates hydroxyl radicals ($OH^•$). Hydroxyl radicals and superoxide radicals and are very powerful oxidants that can decompose organic molecules (the NFA acceptor). Furthermore, direct decomposition of IT-4F through recombination of photogenerated electrons in ZnO and holes in the NFA is possible. The positions of the VB and CB edge of ZnO are crucial to those reactions.[60,61] Through inserting a thin Py-BDP interlayer, we pose a physical barrier between ZnO and IT-4F and an upward shift in the the CBM of ZnO (from 4.0 to 3.7 eV, see Figure 2b), which might disrupt the photocatalytic activity of ZnO (by increasing the energy difference between the CBM of ZnO and HOMO level of IT-4F). Besides the photostability, we also performed aging studies in a batch of five different cells of each type fabricated under identical conditions. The devices were intentionally unencapsulated, whereas they were measured in air every 24 h for a total of 600 h. The devices were kept in dark between measurements. The representative results of these studies are shown in Figure S15. It is deduced that although OSCs based on unmodified ZnO ETLs showed a gradual decrease in all the device characteristics retaining about 50% of the initial PCE for the fullerene and 60% of the initial PCE for the nonfullerene ones, those based on Py-BDP modified ZnO were significantly more stable. They presented less degradation in their performance characteristics hence preserving about 80% of their initial PCE for the same time period.

To gain further insights into the improved photostability of ZnO/Py-BDP-based devices, we investigated the photodegradation of both types of acceptors coated as individual films on pristine and Py-BDP modified ZnO. The absorption spectra of these films before and after their 1 sun illumination were recorded. Figure 7a, b show the normalized absorption spectra of ZnO/IT-4F and ZnO/Py-BDP/IT-4F, respectively, fresh and exposed for 0.5, 3, 5, and 9 h. The absorption spectrum of ZnO/Py-BDP/IT-4F film does not change considerably after 5 h of constant illumination, unlike the absorption of ZnO/IT-4F film, which showed a significant alteration after illumination for the same time. Figure 7c depicts the decrease in the intensity of the absorption maximum of the IT-4F characteristic peak (at ∼700 nm), which is attributed to the π → π* transition and intramolecular charge transfer from the donor to acceptor moiety of IT-4F.[62]

https://dx.doi.org/10.1021/acsami.0c03147
ACS Appl. Mater. Interfaces 2020, 12, 21961−21973

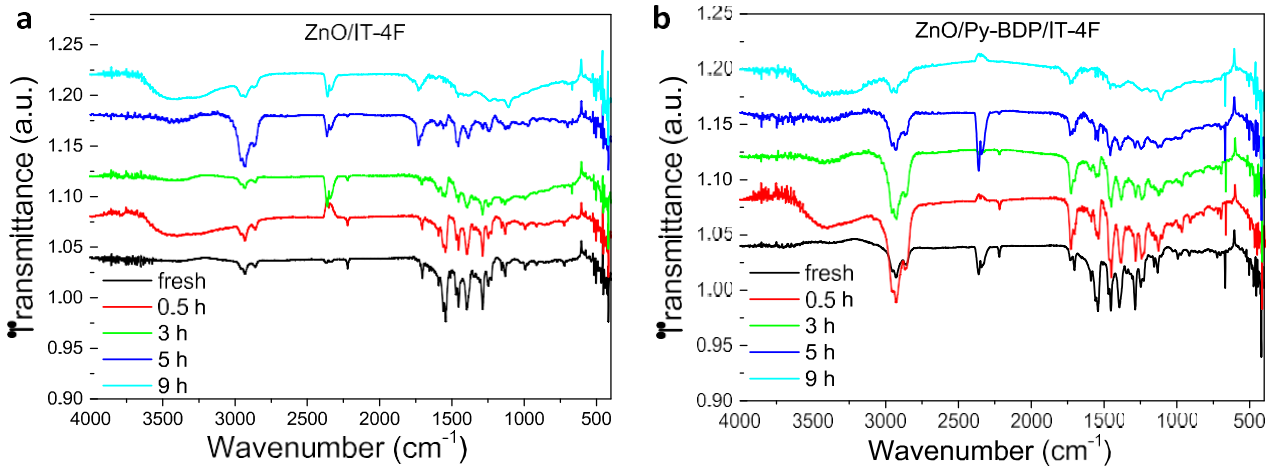

Figure 8. FTIR transmittance spectra of fresh and 1.5 AM light-exposed IT-4F films coated on (a) ZnO and (b) ZnO/Py-BDP substrates.

A more rapid decrease is evident when the NFA is deposited on ZnO substrate. Moreover, the intensity of the shoulder peak around 647 nm is significantly increased for the 5 h exposed ZnO/IT-4F film, indicating that illumination affects more quickly the molecular self-organization in the NFA film deposited on bear ZnO, than in the case of ZnO/Py-BDP/IT-4F sample.[63] Similar results were obtained for $PC_{71}BM$ films coated on the pristine and Py-BDP-modified ZnO substrates (Figure S16). In particular, ZnO/$PC_{71}BM$ films showed a pronounced photodegradation after 5 h of exposure, where a gradual decrease in the intensity of the peak at 375 nm, corresponding to the inter band transition among the π orbitals, was clearly observed (Figure S16a). In contrast, $PC_{71}BM$ film deposited on the ZnO/Py-BDP (Figure S16b) exhibited remarkable photostability. These results indicate that the insertion of Py-BDP on ZnO ETL mitigates photocatalytically induced degradation of NFA and explain the superior photostability of OSCs with the Py-BDP interlayer.

To further investigate the photostability of acceptor films coated on pristine and Py-BDP-modified ZnO substrates, we performed Fourier transform infrared (FTIR) measurements. Figure 8a, b shows the FTIR transmittance spectra of ZnO/IT-4F and ZnO/Py-BDP/IT-4F films, respectively, fresh and exposed to 1.5 AM illumination for 0.5, 3, 5, and 9 h. In both FTIR spectra, peaks at 2218 cm^{-1} (C≡N stretch), and 1704 cm^{-1} (C=O stretch) are observed, as well as the bands between 1591 and 1452 cm^{-1} (C−C_{ring} stretch) and 1246 and 1132 cm^{-1} (C−H_{ring} bend). In addition, a reduction in the intensity of C≡N upon light exposure is evidenced, which in the case of ZnO/IT-4F film took place after only 3 h of exposure and in the ZnO/Py-BDP/IT-4F film was not observed until after 5 h of illumination. A similar trend was noticed for the C−C_{ring} and C−H_{ring} bands in the same time frame. More importantly, the intensity of the peak at 1704 cm^{-1} corresponding to unsaturated carbonyl (C=O) stretching vibrations for the ZnO/IT-4F sample gradually reduced in the span of 3 h, and a new peak appeared at 1730 cm^{-1} attributed to the saturated carbonyl stretching vibrations.[64] On the other hand, in the ZnO/Py-BDP/IT-4F sample, both peaks at 1704 and 1730 cm^{-1} were observed in the exposed sample, revealing a more slower/gradual degradation. The peak at 1704 cm^{-1} finally disappeared only after 9 h of exposure. FTIR measurements were also performed for $PC_{71}BM$ films coated on pristine and Py-BDP-modified ZnO substrates, and the corresponding transmittance spectra are presented in Figure S17. No significant changes in both spectra are observed after exposure for 5 h, in accordance with UV−vis measurements (Figure S16), indicating that $PC_{71}BM$ acceptor is generally more photostable than IT-4F.[65] However, after exposure for 5 h, the intensity of the peak at 699 cm^{-1} corresponding to C−H bond was reduced in the ZnO/$PC_{71}BM$ sample and finally disappeared only after illumination for 9 h, whereas the spectrum of the ZnO/Py-BDP/$PC_{71}BM$ film remained unchanged. These results suggest that Py-BDP can delay the degradation of fullerene and nonfullerene acceptors caused by the photocatalytic activity of the ZnO ETL.

3. CONCLUSIONS

Highly efficient fullerene and nonfullerene OSCs were fabricated using a thin Py-BDP interlayer between the ZnO ETL and the photoactive blend. The introduction of this donor−acceptor dye has induced significant reduction in the W_F of ZnO, hence favoring electron transport toward the cathode. Moreover, it beneficially affected the nanomorphology of the photoactive blend, inducing a higher degree of crystallinity and face-on stacking of the polymer donor molecules within the blend. Accordingly, using the Py-BDP-modified ZnO ETL, PCE values as high as 9.86 and 11.80% were achieved for the fullerene and nonfullerene devices, respectively, which are higher than their pristine ZnO ETL counterparts. In addition, Py-BDP served as a protective layer suppressing the detrimental photodegradation of both types of acceptors, especially of the nonfullerene one, caused by the photocatalytic activity of ZnO upon UV illumination. The photostability of the Py-BDP-modified interface leads to substantially prolonged stable operation of the OSC devices, which is a prerequisite to their future commercialization.

4. EXPERIMENTAL SECTION

Fabrication of Inverted OSCs. Fluorine-doped tin oxide (FTO)-coated glass substrates (Solaronix) were washed by sonication subsequently in deionized water, acetone, and isopropyl alcohol for 10 min each. A thin film (~50 nm) of ZnO was applied on the FTO cathode electrode using solution-processing followed by thermal annealing at 250 °C for 20 min. Particularly, the ZnO film was deposited by a 0.5 Mmol L^{-1} ZnO sol−gel that was prepared using zinc acetate dihydrate in a mixture of ethanolamine and 2-methoxyethanol through spin-coating at 6000 rpm for 40 s. Py-BDP was then spin-coated on ZnO to act as surface modifier of ETL from a

https://dx.doi.org/10.1021/acsami.0c03147
ACS Appl. Mater. Interfaces 2020, 12, 21961−21973

0.35 mg mL^{-1} methanol solution at 2000 rpm for 40 s. Note that prior to deposition, Py-BDP solution was filtered by a 0.22 μm Millipore filter. The photoactive layers of the fullerene and nonfullerene OSCs deposited on pristine or Py-BDP-coated ZnO consisted of either PTB7-Th:$PC_{71}BM$ or PM6:IT-4F blends, respectively. In particular, PTB7-Th:$PC_{71}BM$ blends were dissolved in 1,2-dichlorobenzene, adding also 3 v/v% 1,8-diiodooctane (DIO) having a concentration of 10:15 mg mL^{-1}, and then spin-coated in an argon-filled glovebox at 1000 rpm for 90 s to form uniform films, which were left to dry for 30 min. On the other hand, PM6:IT-4F blended films were spin-coated from a 10:10 mg mL^{-1} chloroform solution, containing a 0.5% per volume DIO, at 2500 rpm for 60 s. Then, the prepared films were placed on a hot plate at 100 °C for 10 min (also in an argon-filled glovebox). Subsequently, MoO_x films acting as hole-transport layers (HTLs) were deposited on the photoactive films using a hot-wire vapor deposition system. Finally, the top electrode consisting of Al was thermally evaporated under a high vacuum (~1 × 10^{-6} Torr) through a shadow mask forming an active area of 12.56 mm^2.

Characterization Techniques. In respect to the electrical characterization of the fabricated OSCs, $J-V$ measurements were performed using a Keithley 2400 source-measure unit under light illumination, where the illumination source was a Xe lamp including an AM 1.5G filter. The calibration of the solar simulator to 1 sun (100 mW cm^{-2}) was performed with a Newport meter. EQE spectra were recorded using an Autolab PGSTAT-30 potensiostat, equipped with an Oriel 1/8 monochromator and a 300 W Xe lamp. GIWAXS patterns were acquired by beamline BL16B1 (Shanghai Synchrotron Radiation Facility). UPS measurements were made using the He I (21.2 eV) excitation line. A voltage of 12.23 V was applied to the specimen in order to separate the high BE cutoff from the analyzer (Leybold EA-11). A Perkin Elmer Lambda UV−vis spectrometer was used to record UV−vis absorption and transmittance spectra of modified or not metal oxide films, as well as organic blended layers coated on top of them. FTIR transmittance measurements were carried out for both pristine and Py-BDP-coated ZnO samples, along with the different photoactive overlayers using a Bruker Tensor 27 FTIR spectrometer having a DTGS detector.

NMR Experiments. One- and two-dimensional NMR spectra were recorded on either Bruker Avance 500 MHz or Bruker Avance III 250 MHz spectrometers as solutions in $CDCl_3$ using the residual solvent signal as the internal standard and were processed with Topspin 4.0.8. A solution of Py-BDP in $CDCl_3$ (0.5 mg/mL) and a concentrated solution of IT-4F (50 mg/mL) were prepared. The solution with IT-4F was then added in a small aliquot (5 μL for addition of 0.25 mg/mL), to reach the final Py-BDP/IT-4F ratio as used for photovoltaic cells. Binding constants (K) were estimated from nonlinear least-squares fitting of the NMR titration data using the suitable equation for 1:1 binding of Py-BDP with IT-4F.[66]

$$\Delta\delta = (\Delta\delta_{max}/[H]_0)(0.5[G]_0 + 0.5([H]_0 + 1/K) - (0.5([G]_0^2 + (2[G]_0(1/K - [H]_0)) + (1/K + [H]_0)^2)^{0.5})) \quad (1)$$

where Δδ is the chemical shift change (in ppm) of pyrene H_{12} on Py-BDP at $[G]_0$, $\Delta\delta_{max}$ is the chemical shift change of the H_{12} resonance when the guest is completely complexed, and $[H]_0$ is the fixed initial concentration of IT-4F. The optimization of interactions between Py-BDP and IT-4F based on NMR data was carried out using Avogadro software (version 1.20).[67,68] The calculations were performed at the Molecular Mechanics (MM) level of theory and Universal Force Fields (UFF) using Steepest descent as local algorithm. This minimum energy representation resulted from three different conformations depending on the distance between the pyrene part of Py-BDP and the difluoro phenyl ring of IT-4F.

ASSOCIATED CONTENT

Supporting Information

The Supporting Information is available free of charge at https://pubs.acs.org/doi/10.1021/acsami.0c03147.

Figure S1−S17 and Table S1 regarding the synthetic procedure, theoretical calculations, absorption and emission measurements, proton NMR studies, estimation of surface energy, additional device measurements, and stability studies (PDF)

AUTHOR INFORMATION

Corresponding Author

Maria Vasilopoulou − *Institute of Nanoscience and Nanotechnology, National Center for Scientific Research Demokritos, Athens 15310, Greece;* orcid.org/0000-0001-8893-1691; Email: m.vasilopoulou@inn.demokritos.gr

Authors

Anastasia Soultati − *Institute of Nanoscience and Nanotechnology, National Center for Scientific Research Demokritos, Athens 15310, Greece*

Apostolis Verykios − *Institute of Nanoscience and Nanotechnology, National Center for Scientific Research Demokritos, Athens 15310, Greece; Department of Physics, University of Patras, Patras 26504, Greece*

Stylianos Panagiotakis − *Institute of Nanoscience and Nanotechnology, National Center for Scientific Research Demokritos, Athens 15310, Greece*

Konstantina-Kalliopi Armadorou − *Institute of Nanoscience and Nanotechnology, National Center for Scientific Research Demokritos, Athens 15310, Greece; Department of Chemistry, National and Kapodestrian University of Athens, Zografos 15771, Greece*

Muhammad Irfan Haider − *Department of Physics, University of Konstanz, Konstanz 78457, Germany; Department of Chemistry, University of Wah, Wah 47040, Pakistan*

Andreas Kaltzoglou − *Institute of Nanoscience and Nanotechnology, National Center for Scientific Research Demokritos, Athens 15310, Greece;* orcid.org/0000-0002-3093-9778

Charalampos Drivas − *Department of Chemical Engineering, University of Patras, Patras 26504, Greece*

Azhar Fakharuddin − *Department of Physics, University of Konstanz, Konstanz 78457, Germany*

Xichang Bao − *Qingdao Institute of Bioenergy and Bioprocess Technology, Chinese Academy of Sciences, Qingdao 266101, China;* orcid.org/0000-0001-7325-7550

Chunming Yang − *Shanghai Synchrotron Radiation Facility, Shanghai Advanced Research Institute, Chinese Academy of Sciences, Shanghai 201204, China;* orcid.org/0000-0001-8008-3675

Abd. Rashid bin Mohd Yusoff − *Department of Physics, Vivian Tower, Singleton Park, Swansea University, Swansea SA2 8PP, United Kingdom*

Evangelos K. Evangelou − *Department of Physics, University of Ioannina, Ioannina 45110, Greece*

Ioannis Petsalakis − *Theoretical and Physical Chemistry Institute, National Hellenic Research Foundation, Athens 11635, Greece*

Stella Kennou − *Department of Chemical Engineering, University of Patras, Patras 26504, Greece*

Polycarpos Falaras − *Institute of Nanoscience and Nanotechnology, National Center for Scientific Research Demokritos, Athens 15310, Greece;* orcid.org/0000-0002-9553-5301

https://dx.doi.org/10.1021/acsami.0c03147
ACS Appl. Mater. Interfaces 2020, 12, 21961−21973

Konstantina Yannakopoulou − *Institute of Nanoscience and Nanotechnology, National Center for Scientific Research Demokritos, Athens 15310, Greece*

George Pistolis − *Institute of Nanoscience and Nanotechnology, National Center for Scientific Research Demokritos, Athens 15310, Greece;* orcid.org/0000-0002-0704-4802

Panagiotis Argitis − *Institute of Nanoscience and Nanotechnology, National Center for Scientific Research Demokritos, Athens 15310, Greece;* orcid.org/0000-0001-7070-2006

Complete contact information is available at: https://pubs.acs.org/10.1021/acsami.0c03147

Notes

The authors declare no competing financial interest.

ACKNOWLEDGMENTS

Support of this work by the project "Development of Materials and Devices for Industrial, Health, Environmental and Cultural Applications" (MIS 5002567) which is implemented under the "Action for the Strategic Development on the Research and Technological Sector", funded by the Operational Programme "Competitiveness, Entrepreneurship and Innovation" (NSRF 2014-2020) and cofinanced by Greece and the European Union (European Regional Development Fund), is acknowledged.

REFERENCES

(1) Forrest, S. R. The Path to Ubiquitous and Low-Cost Organic Electronic Appliances on Plastic. *Nature* 2004, *428*, 911−918.

(2) Krebs, F. C. Fabrication and Processing of Polymer Solar Cells: A Review of Printing and Coating Techniques. *Sol. Energy Mater. Sol. Cells* 2009, *93*, 394−412.

(3) He, Z.; Xiao, B.; Liu, F.; Wu, H.; Yang, Y.; Xiao, S.; Wang, C.; Russell, T. P.; Cao, Y. Single-Junction Polymer Solar Cells with High Efficiency and Photovoltage. *Nat. Photonics* 2015, *9*, 174−179.

(4) Li, G.; Zhu, R.; Yang, Y. Polymer Solar Cells. *Nat. Photonics* 2012, *6*, 153−161.

(5) Cheng, P.; Bai, H.; Zawacka, N. K.; Andersen, T. R.; Liu, W.; Bundgaard, E.; Jørgensen, M.; Chen, H.; Krebs, F. C.; Zhan, X. Roll-Coated Fabrication of Fullerene-Free Organic Solar Cells with Improved Stability. *Adv. Sci.* 2015, *2*, 1500096.

(6) Che, X. Z.; Xiao, X.; Zimmerman, J. D.; Fan, D. J.; Forrest, S. R. High-Efficiency, Vacuum-Deposited, Small-Molecule Organic Tandem and Triple-Junction Photovoltaic Cells. *Adv. Energy Mater.* 2014, *4*, 1400568.

(7) Chen, C. C.; Chang, W. H.; Yoshimura, K.; Ohya, K.; You, J. B.; Gao, J.; Hong, Z. R.; Yang, Y. An Efficient Triple-Junction Polymer Solar Cell having a Power Conversion Efficiency Exceeding 11%. *Adv. Mater.* 2014, *26*, 5670.

(8) Li, N.; Baran, D.; Forberich, K.; Machui, F.; Ameri, T.; Turbiez, M.; Carrasco-Orozco, M.; Drees, M.; Facchetti, A.; Krebs, F. C.; Brabec, C. J. Towards 15% Energy Conversion Efficiency: a Systematic Study of the Solution-Processed Organic Tandem Solar Cells based on Commercially Available Materials. *Energy Environ. Sci.* 2013, *6*, 3407−3413.

(9) Lin, Y.; Firdaus, Y.; Nugraha, M. I.; Liu, F.; Karuthedath, S.; Emwas, A.-H.; Zhang, W.; Seitkhan, A.; Neophytou, M.; Faber, H.; Yengel, E.; McCulloch, I.; Tsetseris, L.; Laquai, F.; Anthopoulos, T. D. 17.1% Efficient Single-Junction Organic Solar Cells Enabled by n-Type Doping of the Bulk-Heterojunction. *Advanced Science* 2020, *7*, 1903419.

(10) Meng, L.; Zhang, W.; Wan, X.; Li, C.; Zhang, X.; Wang, Y.; Ke, X.; Xiao, Z.; Ding, L.; Xia, R.; Yip, H.-L.; Cao, Y.; Chen, Y. Organic and Solution-Processed Tandem Solar Cells with 17.3% Efficiency. *Science* 2018, *361*, 1094−1098.

(11) Wadsworth, A.; Moser, M.; Marks, A.; Little, M. S.; Gasparini, N.; Brabec, C. J.; Baran, D.; McCulloch, I. Critical Review of the Molecular Design Progress in Non-Fullerene Electron Acceptors Towards Commercially Viable Organic Solar Cells. *Chem. Soc. Rev.* 2019, *48*, 1596−1625.

(12) Sun, H.; Chen, F.; Chen, Z.-K. Recent Progress on Non-Fullerene Acceptors for Organic Photovoltaics. *Mater. Today* 2019, *24*, 94−118.

(13) Zhang, G.; Zhao, J.; Chow, P. C. Y.; Jiang, K.; Zhang, J.; Zhu, Z.; Zhang, J.; Huang, F.; Yan, H. Nonfullerene Acceptor Molecules for Bulk Heterojunction Organic Solar Cells. *Chem. Rev.* 2018, *118* (7), 3447−3507.

(14) Yan, C.; Barlow, S.; Wang, Z.; Yan, H.; Jen, A. K.-Y.; Marder, S. R.; Zhan, X. Non-Fullerene Acceptors for Organic Solar Cells. *Nat. Rev. Mater.* 2018, *3*, 1−8.

(15) Baran, D.; Kirchartz, T.; Wheeler, S.; Dimitrov, S.; Abdelsamie, M.; Gorman, J.; Ashraf, R. S.; Holliday, S.; Wadsworth, A.; Gasparini, N.; Kaienburg, P.; Yan, H.; Amassian, A.; Brabec, C. J.; Durrant, J. R.; McCulloch, I. Reduced Voltage Losses Yield 10% Efficient Fullerene Free Organic Solar Cells with > 1 V Open Circuit Voltages. *Energy Environ. Sci.* 2016, *9*, 3783−3793.

(16) Hou, J.; Inganas, O.; Friend, R. H.; Gao, F. Organic Solar Cells based on Non-Fullerene Acceptors. *Nat. Mater.* 2018, *17*, 119−128.

(17) Liu, F.; Hou, T.; Xu, X.; Sun, L.; Zhou, J.; Zhao, X.; Zhang, S. Recent Advances in Nonfullerene Acceptors for Organic Solar Cells. *Macromol. Rapid Commun.* 2018, *39*, 1700555.

(18) Ma, H.; Yip, H.-L.; Huang, F.; Jen, A.K.-Y. Interface Engineering for Organic Electronics. *Adv. Funct. Mater.* 2010, *20*, 1371−1388.

(19) Walker, B.; Choi, H.; Kim, J. Y. Interfacial Engineering for Highly Efficient Organic Solar Cells. *Curr. Appl. Phys.* 2017, *17*, 370−391.

(20) Yi, C.; Hu, X.; Gong, X.; Elzatahry, A. Interfacial Engineering for High Performance Organic Photovoltaics. *Mater. Today* 2016, *19*, 169−177.

(21) Li, G.; Shrotriya, V.; Huang, J. S.; Yao, Y.; Moriarty, T.; Emery, K.; Yang, Y. High-Efficiency Solution Processable Polymer Photovoltaic Cells by Self-Organization of Polymer Blends. *Nat. Mater.* 2005, *4*, 864.

(22) Lai, T.-H.; Tsang, S.-W.; Manders, J. R.; Chen, S.; So, F. Properties of Interlayer for Organic Photovoltaics. *Mater. Today* 2013, *16*, 424−432.

(23) Park, J. H.; Lee, T.-W.; Chin, B.-D.; Wang, D. H.; Park, O. O. Roles of Interlayers in Efficient Organic Photovoltaic Devices. *Macromol. Rapid Commun.* 2010, *31*, 2095−2108.

(24) Yin, Z.; Wei, J.; Zheng, Q. Interfacial Materials for Organic Solar Cells: Recent Advances and Perspectives. *Adv. Sci.* 2016, *3*, 1500362.

(25) Yan, Y.; Cai, F.; Yang, L.; Li, J.; Zhang, Y.; Qin, F.; Xiong, C.; Zhou, Y.; Lidzey, D. G.; Wang, T. Light-Soaking-Free Inverted Polymer Solar Cells with an Efficiency of 10.5% by Compositional and Surface Modifications to a Low-Temperature-Processed TiO_2 Electron-Transport Layer. *Adv. Mater.* 2017, *29*, 1604044.

(26) Nam, M.; Huh, J. Y.; Park, Y.; Hong, Y. C.; Ko, D.-H. Interfacial Modification Using Hydrogenated TiO_2 Electron-Selective Layers for High-Efficiency and Light-Soaking-Free Organic Solar Cells. *Adv. Energy Mater.* 2018, *8*, 1703064.

(27) Vasilopoulou, M. The Effect of Surface Hydrogenation of Metal Oxides on the Nanomorphology and the Charge Generation Efficiency of Polymer Blend Solar Cells. *Nanoscale* 2014, *6*, 13726−13739.

(28) Bai, S.; Jin, Y.; Liang, X.; Ye, Z.; Wu, Z.; Sun, B.; Ma, Z.; Tang, Z.; Wang, J.; Würfel, U.; Gao, F.; Zhang, F. Ethanedithiol Treatment of Solution-Processed ZnO Thin Films: Controlling the Intragap States of Electron Transporting Interlayers for Efficient and Stable Inverted Organic Photovoltaics. *Adv. Energy Mater.* 2015, *5*, 1401606.

(29) Richardson, B. J.; Wang, X.; Almutairi, A.; Yu, Q. High Efficiency PTB7-based Inverted Organic Photovoltaics on Nano-

Ridged and Planar Zinc Oxide Electron Transport Layers. *J. Mater. Chem. A* 2015, *3*, 5563−5571.
(30) Schmidt-Mende, L.; MacManus-Driscoll, J. L. ZnO − Nanostructures, Defects, and Devices. *Mater. Today* 2007, *10*, 40−48.
(31) Soultati, A.; Verykios, A.; Speliotis, T.; Fakis, M.; Sakellis, I.; Jaouani, H.; Davazoglou, D.; Argitis, P.; Vasilopoulou, M. Organic Solar Cells of Enhanced Efficiency and Stability using Zinc Oxide:Zinc Tungstate Nanocomposite as Electron Extraction Layer. *Org. Electron.* 2019, *71*, 227−237.
(32) Soultati, A.; Fakharuddin, A.; Polydorou, E.; Drivas, C.; Kaltzoglou, A.; Haider, I. M.; Kournoutas, F.; Fakis, M.; Palilis, L. C.; Kennou, S.; Davazoglou, D.; Falaras, P.; Argitis, P.; Gardelis, S.; Kordatos, A.; Chroneos, A.; Schmidt-Mende, L.; Vasilopoulou, M. Lithium Doping of ZnO for High Efficiency and Stability Fullerene and Non-fullerene Organic Solar Cells. *ACS Appl. Energy Mater.* 2019, *2*, 1663−1675.
(33) Ou, K.-L.; Ehamparam, R.; MacDonald, G.; Stubhan, T.; Wu, X.; Shallcross, R. C.; Richards, R.; Brabec, C. J.; Saavedra, S. S.; Armstrong, N. R. Characterization of ZnO Interlayers for Organic Solar Cells: Correlation of Electrochemical Properties with Thin-Film Morphology and Device Performance. *ACS Appl. Mater. Interfaces* 2016, *8*, 19787−19798.
(34) Wang, L.; Zheng, Y.; Li, X.; Dong, W.; Tang, W.; Chen, B.; Li, C.; Li, X.; Zhang, T.; Xu, W. Nanostructured Porous ZnO Film with Enhanced Photocatalytic Activity. *Thin Solid Films* 2011, *519*, 5673−5678.
(35) Polydorou, E.; Botzakaki, M.; Drivas, C.; Seintis, K.; Sakellis, I.; Soultati, A.; Kaltzoglou, A.; Speliotis, T.; Fakis, M.; Palilis, L. C.; Kennou, S.; Fakharuddin, A.; Schmidt-Mende, L.; Davazoglou, D.; Falaras, P.; Argitis, P.; Krontiras, C. A.; Georga, S. N.; Vasilopoulou, M. Insights into the Passivation Effect of Atomic Layer Deposited Hafnium Oxide for Efficiency and Stability Enhancement in Organic Solar Cells. *J. Mater. Chem. C* 2018, *6*, 8051−8059.
(36) Hu, L.; Liu, Y.; Mao, L.; Xiong, S.; Sun, L.; Zhao, N.; Qin, F.; Jiang, Y.; Zhou, Y. Chemical Reaction between ITIC Electron Acceptor and Amine-containing Interfacial Layer in Non-Fullerene Solar Cells. *J. Mater. Chem. A* 2018, *6*, 2273−2278.
(37) Jiang, Y.; Sun, L.; Jiang, F.; Xie, C.; Hu, L.; Dong, X.; Qin, F.; Liu, T.; Hu, L.; Jiang, X.; Zhou, Y. Photocatalytic Effect of ZnO on Nonfullerene Acceptors and its Mitigation by SnO_2 for Nonfullerene Organic Solar Cells. *Mater. Horiz.* 2019, *6*, 1438−1443.
(38) Woo, S.; Hyun Kim, W.; Kim, H.; Yi, Y.; Lyu, H.-K.; Kim, Y. 8.9% Single-Stack Inverted Polymer Solar Cells with Electron-Rich Polymer Nanolayer-Modified Inorganic Electron-Collecting Buffer Layers. *Adv. Energy Mater.* 2014, *4*, 1301692.
(39) Tountas, M.; Verykios, A.; Polydorou, E.; Kaltzoglou, A.; Soultati, A.; Balis, N.; Angaridis, P. A.; Papadakis, M.; Nikolaou, V.; Auras, F.; Palilis, L. C.; Tsikritzis, D.; Evangelou, E. K.; Gardelis, S.; Koutsoureli, M.; Papaioannou, G.; Petsalakis, I. D.; Kennou, S.; Davazoglou, D.; Argitis, P.; Falaras, P.; Coutsolelos, A. G.; Vasilopoulou, M. Engineering of Porphyrin Molecules for Use as Effective Cathode Interfacial Modifiers in Organic Solar Cells of Enhanced Efficiency and Stability. *ACS Appl. Mater. Interfaces* 2018, *10* (24), 20728−20739.
(40) Ha, Y. E.; Jo, M. Y.; Park, J.; Kang, Y. C.; Yoo, S. I.; Kim, J. H. Inverted Type Polymer Solar Cells with Self-Assembled Monolayer Treated ZnO. *J. Phys. Chem. C* 2013, *117*, 2646.
(41) Song, C. E.; Ryu, K. Y.; Hong, S. J.; Bathula, C.; Lee, S. K.; Shin, W. S.; Lee, J. C.; Choi, S. K.; Kim, J. H.; Moon, S. J. Enhanced Performance in Inverted Polymer Solar Cells with D−π−A-Type Molecular Dye Incorporated on ZnO Buffer Layer. *ChemSusChem* 2013, *6*, 1445.
(42) Lee, B. R.; Choi, H.; SunPark, J.; Lee, H. J.; Kim, S. O.; Kim, J. Y.; Song, M. H. Surface Modification of Metal Oxide using Ionic Liquid Molecules in Hybrid Organic−Inorganic Optoelectronic Devices. *J. Mater. Chem.* 2011, *21*, 2051.
(43) Yu, W.; Huang, L.; Yang, D.; Fu, P.; Zhou, L.; Zhang, J.; Li, C. Efficiency Exceeding 10% for Inverted Polymer Solar Cells with a ZnO/Ionic Liquid Combined Cathode Interfacial Layer. *J. Mater. Chem. A* 2015, *3*, 10660.
(44) Yu, W.; Zhou, L.; Yu, S.; Fu, P.; Guo, X.; Li, C. Ionic Liquids with Variable Cations as Cathode Interlayer for Conventional Polymer Solar Cells. *Org. Electron.* 2017, *42*, 387−392.
(45) Li, C.-Z.; Chang, C.-Y.; Zang, Y.; Ju, H.-X.; Chueh, C.-C.; Liang, P.-W.; Cho, N.; Ginger, D. S.; Jen, A. K. Y. Suppressed Charge Recombination in Inverted Organic Photovoltaics via Enhanced Charge Extraction by Using a Conductive Fullerene Electron Transport Layer. *Adv. Mater.* 2014, *26*, 6262−6267.
(46) Zhen, J.; Liu, Q.; Chen, X.; Li, D.; Qiao, Q.; Lu, Y.; Yang, S. An Ethanolamine-Functionalized Fullerene as an Efficient Electron Transport Layer for High-Efficiency Inverted Polymer Solar Cells. *J. Mater. Chem. A* 2016, *4*, 8072−8079.
(47) Liu, J.; Li, J.; Tu, G. Ether Chain Functionalized Fullerene Derivatives as Cathode Interface Materials for Efficient Organic Solar Cells. *Front. Optoelectron.* 2018, *11*, 348−359.
(48) Guo, J.; Li, Z.; Wang, M.; Sun, Y.; Fu, D.; Liu, C.; Guo, W. Fullerene Derivative Layer Induced Phase Separation and Charge Transport Improvement for Inverted Polymer Solar Cells. *Thin Solid Films* 2019, *690*, 137559.
(49) Li, N.; McCulloch, I.; Brabec, C. J. Analyzing the Efficiency, Stability and Cost Potential for Fullerene-Free Organic Photovoltaics in One Figure of Merit. *Energy Environ. Sci.* 2018, *11*, 1355−1361.
(50) Polydorou, E.; Sakellis, I.; Soultati, A.; Kaltzoglou, A.; Papadopoulos, T. A.; Briscoe, J.; Tsikritzis, D.; Fakis, M.; Palilis, L. C.; Kennou, S.; Argitis, P.; Falaras, P.; Davazoglou, D.; Vasilopoulou, M. Avoiding Ambient air and Light Induced Degradation in High-Efficiency Polymer Solar Cells by the use of Hydrogen-Doped zinc oxide as Electron Extraction Material. *Nano Energy* 2017, *34*, 500−514.
(51) Zhao, J.; Li, Y.; Lin, H.; Liu, Y.; Jiang, K.; Mu, C.; Ma, T.; Lin Lai, J. Y.; Hu, H.; Yu, D.; Yan, H. High-Efficiency Non-Fullerene Organic Solar Cells Enabled by a Difluoro benzothiadiazole-based Donor Polymer Combined with a Properly Matched Small Molecule Acceptor. *Energy Environ. Sci.* 2015, *8*, 520−525.
(52) Dobkowski, J.; Rettig, W.; Waluk, J. Intramolecular Charge-Transfer Properties of a Molecule with a Large Donor Group: The Case of 4′-(Pyren-1-yl)Benzonitrile. *Phys. Chem. Chem. Phys.* 2002, *4*, 4334−4339.
(53) Papamakarios, V.; Polydorou, E.; Soultati, A.; Droseros, N.; Tsikritzis, D.; Douvas, A. M.; Palilis, L.; Fakis, M.; Kennou, S.; Argitis, P.; Vasilopoulou, M. Surface Modification of ZnO Layers via Hydrogen Plasma Treatment for Efficient Inverted Polymer Solar Cells. *ACS Appl. Mater. Interfaces* 2016, *8*, 1194−1205.
(54) Liu, J.; Shao, S.; Fang, G.; Meng, B.; Xie, Z.; Wang, L. High-Efficiency Inverted Polymer Solar Cells with Transparent and Work-Function Tunable MoO_3-Al Composite Film as Cathode Buffer Layer. *Adv. Mater.* 2012, *24*, 2774−2779.
(55) Nandy, R.; Subramoni, M.; Varghese, B.; Sankararaman, S. Intramolecular π-Stacking Interaction in a Rigid Molecular Hinge Substituted with 1-(Pyrenylethynyl) Units. *J. Org. Chem.* 2007, *72*, 938−944.
(56) Hsieh, Y.-J.; Huang, Y.-C.; Liu, W.-S.; Su, Y.-A.; Tsao, C.-C.; Rwei, S.-P.; Wang, L. Insights into the Morphological Instability of Bulk Heterojunction PTB7-Th/PCBM Solar Cells upon High-Temperature Aging. *ACS Appl. Mater. Interfaces* 2017, *9* (17), 14808−14816.
(57) Yang, X.; Zheng, F.; Xu, W.; Bi, P.; Feng, L.; Liu, J.; Hao, X. Improving the Compatibility of Donor Polymers in Efficient Ternary Organic Solar Cells via Post-Additive Soaking Treatment. *ACS Appl. Mater. Interfaces* 2017, *9* (1), 618−627.
(58) Zhang, L.; Zhao, H.; Lin, B.; Yuan, J.; Xu, X.; Wu, J.; Zhou, K.; Guo, X.; Zhang, M.; Ma, W. A Blade-Coated Highly Efficient Thick Active Layer for Non-Fullerene Organic Solar Cells. *J. Mater. Chem. A* 2019, *7*, 22265−22273.
(59) Liu, T.; Luo, Z.; Fan, Q.; Zhang, G.; Zhang, L.; Gao, W.; Guo, X.; Ma, W.; Zhang, M.; Yang, C.; Li, Y.; Yan, H. Use of Two Structurally Similar Small Molecular Acceptors Enabling Ternary

https://dx.doi.org/10.1021/acsami.0c03147
ACS Appl. Mater. Interfaces 2020, 12, 21961−21973

Organic Solar Cells with High Efficiencies and Fill Factors. *Energy Environ. Sci.* 2018, *11*, 3275−3282.
(60) Mousavi, S. L.; Jamali-Sheini, F.; Sabaeian, M.; Yousefi, R. Enhanced Solar Cell Performance of P3HT:PCBM by SnS Nanoparticles. *Sol. Energy* 2020, *199*, 872−884.
(61) Azarang, M.; Aliahmad, M.; Ghorban Shiravizadeh, A.; Azimi, H. R.; Yousefi, R. Zn-doped PbO Nanoparticles (NPs)/Fluorine-doped Tin Oxide (FTO) as Photoanode for Enhancement of Visible-Near-Infrared (NIR) Broad Spectral Photocurrent Application of Narrow Bandgap Nanostructures: SnSe NPs as a Case Study. *J. Appl. Phys.* 2018, *124*, 123101.
(62) Zhao, W.; Li, S.; Yao, H.; Zhang, S.; Zhang, Y.; Yang, B.; Hou, J. Molecular Optimization Enables over 13% Efficiency in Organic Solar Cells. *J. Am. Chem. Soc.* 2017, *139*, 7148−7151.
(63) Lin, Y.; Wang, J.; Zhang, Z. G.; Bai, H.; Li, Y.; Zhu, D.; Zhan, X. An Electron Acceptor Challenging Fullerenes for Efficient Polymer Solar Cells. *Adv. Mater.* 2015, *27*, 1170.
(64) Silverstein, M. R.; Webster, X. F.; Kiemle, J. D. *Spectrometric Identification of Organic Compounds*, 7th ed.; John Wiley & Sons: New York, 2005; Chapter 2, pp 72−110.
(65) Doumon, N. Y.; Dryzhov, M. V.; Houard, F. V.; Le Corre, V. M.; Rahimi Chatri, A.; Christodoulis, P.; Koster, L. J. A. Photostability of Fullerene and Non-Fullerene Polymer Solar Cells: The Role of the Acceptor. *ACS Appl. Mater. Interfaces* 2019, *11*, 8310−8318.
(66) Thordarson, P. Determining Association Constants from Titration Experiments in Supramolecular Chemistry. *Chem. Soc. Rev.* 2011, *40*, 1305−1323.
(67) *Avogadro: An Open-source Molecular Builder and Visualization Tool*, version 1.20; http://avogadro.cc/.
(68) Hanwell, M. D.; Curtis, D. E.; Lonie, D. C.; Vandermeersch, T.; Zurek, E.; Hutchison, G. R. Avogadro: An Advanced Semantic Chemical Editor, Visualization, and Analysis Platform. *J. Cheminf.* 2012, *4*, 17.

https://dx.doi.org/10.1021/acsami.0c03147
ACS Appl. Mater. Interfaces 2020, 12, 21961−21973